Effect of ocean surface currents on wind stress, heat flux, and wind power input to the ocean

Jordan T. Dawe[1] and LuAnne Thompson[1]

Received 17 January 2006; revised 27 March 2006; accepted 31 March 2006; published 6 May 2006.

[1] The effect of ocean surface currents on bulk algorithm calculations of wind stress and heat flux in a 1/5° resolution model of the North Pacific is investigated. Two year-long model runs are performed, one with wind speed modified by ocean surface velocities and one without. Basin averaged heat flux and wind stress differences between the models were only 1–2%, but localized flux reductions of ~10% were found in the tropics and in the Kuroshio current system. Basin average power input by the wind to the general circulation was reduced by 27% when the effect of surface currents was included. Tropical surface currents were reduced by 10%, tropical surface temperature warmed by 0.1°C, and equatorial upwelling was reduced by 15% due to the changed velocity field. **Citation:** Dawe, J. T., and L. Thompson (2006), Effect of ocean surface currents on wind stress, heat flux, and wind power input to the ocean, *Geophys. Res. Lett.*, *33*, L09604, doi:10.1029/2006GL025784.

1. Introduction

[2] Bulk formula parameterizations of the air-sea transfer of heat and momentum are a vital part of the quest for realistic simulation of the atmosphere-ocean system. These parameterizations share a similar mathematical structure; they assume that air-sea fluxes can be represented by relationships of the form:

$$\boldsymbol{\tau} = \rho_a C_d |\mathbf{u}_a - \mathbf{u}_s|(\mathbf{u}_a - \mathbf{u}_s) \tag{1a}$$

$$Q_s = \rho_a c_{pa} C_h |\mathbf{u}_a - \mathbf{u}_s|(\theta_a - \theta_s) \tag{1b}$$

$$Q_l = \rho_a L_e C_e |\mathbf{u}_a - \mathbf{u}_s|(q_a - q_s) \tag{1c}$$

where ρ_a is the air density, c_{pa} is the specific heat of air, L_e is the latent heat of evaporation of water, C_d, C_h, and C_e are the transfer coefficients for stress, sensible heat, and latent heat respectively, $\mathbf{u}_a - \mathbf{u}_s$ is the wind velocity relative to the ocean surface velocity, $\theta_a - \theta_s$ and $q_a - q_s$ are the differences in potential temperature and humidity between the ocean surface and the atmosphere, respectively, and Q is positive if it causes oceanic warming. Equation (1c) is also used to calculate the evaporation rate, Q_l/L_e. The various bulk formulae [*Large and Pond*, 1982; *Fairall et al.*, 1996; *Zeng et al.*, 1998] differ mainly in the methods used to calculate C_d, C_h, and C_e, which vary with the strength of atmospheric boundary layer turbulence.

[1]Department of Oceanography, University of Washington, Seattle, Washington, USA.

0094-8276/06/2006GL025784$05.00

[3] In general practice the relative motion of the surface currents is assumed to have a negligible effect on air-sea flux and $\mathbf{u}_s$ is set to zero. However, two model studies have examined this approximation and found that surface currents significantly modify air-sea interaction in regions where winds are weak and surface currents are strong. *Pacanowski* [1987] shows that including the effect of surface currents in a simulation of the tropical Atlantic reduces the equatorial current speed by 30%, which has impacts on upwelling and sea surface temperature (SST) along the equator. More recently, *Luo et al.* [2005] find that allowing ocean current relative motion to reduce wind stress improves the simulation of SST in the western Equatorial Pacific.

[4] The advent of scatterometer-based wind products has allowed the reality of this effect to be confirmed in data. Satellite scatterometers measure microwave backscatter from centimeter scale waves on the ocean surface, which respond to air-sea stress, not air speed. Wind stress derived from scatterometer data naturally accounts for the moving ocean. *Kelly et al.* [2001] find that differences between scatterometer wind speeds and annenometer data from the TAO buoy array are explained by the surface currents measured by the buoys. *Cornillon and Park* [2001] were able to use NSCAT data to calculate the surface velocity field in a warm-core Gulf Stream eddy. Most strikingly, *Chelton et al.* [2004] present 4-year averages of QuikSCAT wind stress curl data in which the Kuroshio and Gulf Stream are clearly visible, as well as numerous other current systems.

[5] However, the greatest impact of ocean surface currents on air-sea interaction may lie in the power input by the mean wind to the ocean. In off-equatorial areas where geostrophy holds, wind power input can be divided into power that is added to the general circulation,

$$P_{circ} = \boldsymbol{\tau} \bullet \mathbf{u}_{geo}, \tag{2a}$$

and power that drives mixing in the upper ocean,

$$P_{ml} = \boldsymbol{\tau} \bullet \mathbf{u}_{Ekman}, \tag{2b}$$

where $\mathbf{u}_{geo}$ is the geostrophic surface current and $\mathbf{u}_{Ekman}$ is the Ekman surface current [*Wang and Huang*, 2004]. Recent work by *Duhaut and Straub* [2006] show that accounting for surface currents in calculations of wind stress in an idealized 3-layer quasi-geostrophic model reduces power input to the geostrophic circulation by 20–35%. *Munk and Wunsch* [1998] estimate that over half of the power needed by ocean mixing processes to maintain the abyssal stratification is supplied by the wind. Because of this, power input errors will become increasingly important in models of the deep circulation as modeling moves toward energy-based mixing parameterizations.

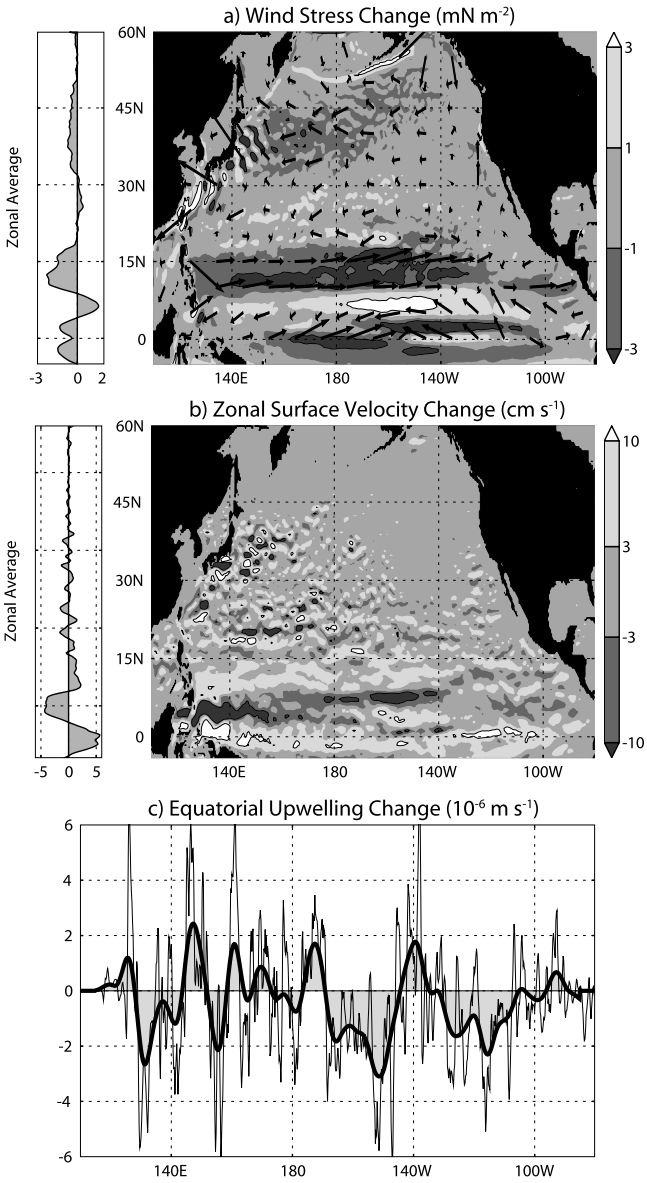

Figure 1. Average (a) wind stress change (in mN m^{-2}, vectors indicate direction), (b) zonal surface velocity change (in m s^{-1}), and (c) vertical entrainment change (averaged from 2.5°S to 2.5°N, in m s^{-1}) when the effect of ocean surface currents on the wind stress is included.

[6] With these concerns in mind, we examine the impact of surface currents on air-sea interaction in a realistic model of the North Pacific.

2. Model Description

[7] This study uses the Hallberg Isopycnal Model [*Hallberg*, 1995; *Ladd and Thompson*, 2002]. HIM is a primitive equation isopycnal model with a fully nonlinear equation of state. The model has realistic topography and is coupled to a variable-density *Oberhuber* [1993] type mixed-layer model, modified to support multiple dynamic layers. The model was configured with 20 isopycnal layers, with 5 of these representing the mixed layer. The model was run at 1/5° resolution over the domain 10°S–60°N, 110°E–80°W. Open northern and southern boundaries are simulated using sponge layers which relax layer thickness, theta and salinity to the Levitus monthly climatology.

[8] Wind, heat and freshwater forcing drive the model. Precipitation and long- and short-wave radiation flux are calculated using average daily values from the NCEP reanalysis. Latent and sensible heat fluxes, wind stress, and evaporation are calculated using the UA bulk formula [*Zeng et al.*, 1998] driven by average daily NCEP 10-meter temperature, humidity, and wind speed. NCEP data from 2001 is used, a year in which the PDO and ENSO indexes are neutral. In addition, surface salinity is relaxed to monthly climatological salinity values on a one-year time scale. Sponge layers at the northern and southern boundaries relax temperature, salinity and layer interface depth to average monthly values to simulate open ocean. All forcing fields are spline-interpolated at each time step.

[9] In order to better represent the Ekman layer, the mixed layer was split into four dynamic layers and a buffer layer that couples the mixed layer to the internal isopycnals. At each time step the temperature and salinity is vertically homogenized in the mixed layer, while momentum is mixed vertically through cross-layer mass fluxes and viscosity.

[10] Power input by the wind was calculated in the model code at each time step. The power input was divided into geostrophic and ageostrophic components by calculating a geostrophic velocity from the model pressure field. This geostrophic velocity was then subtracted from the velocity field to obtain the ageostrophic velocity, which we identify with the Ekman velocity. This division was not performed within 5° of the equator, where the geostrophic relationship breaks down.

[11] Two model runs were performed, one with the effect of ocean surface currents included in the bulk algorithm and one with the ocean surface currents set to zero. This was the only difference between the model runs. The models were spun up for two years with monthly climatological forcing then run for a year with NCEP daily forcing. The output of this year, saved as five-day averages, was analyzed.

[12] The two-year spin up time we used is not long enough for the model to achieve proper equilibrium with the atmospheric forcing. However, it does allow us to model at a much higher horizontal resolution than would otherwise be possible, improving the representation of the mesoscale eddies. It also improves the simulation of the Kuroshio Extension's surface current field, since geostrophic adjustment has not had time to push the Kuroshio separation point northward (a common bias in models with resolution coarser than ~0.1°).

3. Effect of Current Feedback

[13] For our analysis we take differences between the annual means of the run with and the run without surface currents included in the bulk formulas. Including surface currents alters tropical wind stress in a set of zonal bands (Figure 1a) that correspond to the positions of the North Equatorial Current (NEC, 10°N–15°N), the North Equatorial Countercurrent (NECC, 5°N–10°N), and the South Equatorial Current (SEC, 5°S–5°N). Stress differences are concentrated in the tropics, the Kuroshio, and the Kuroshio

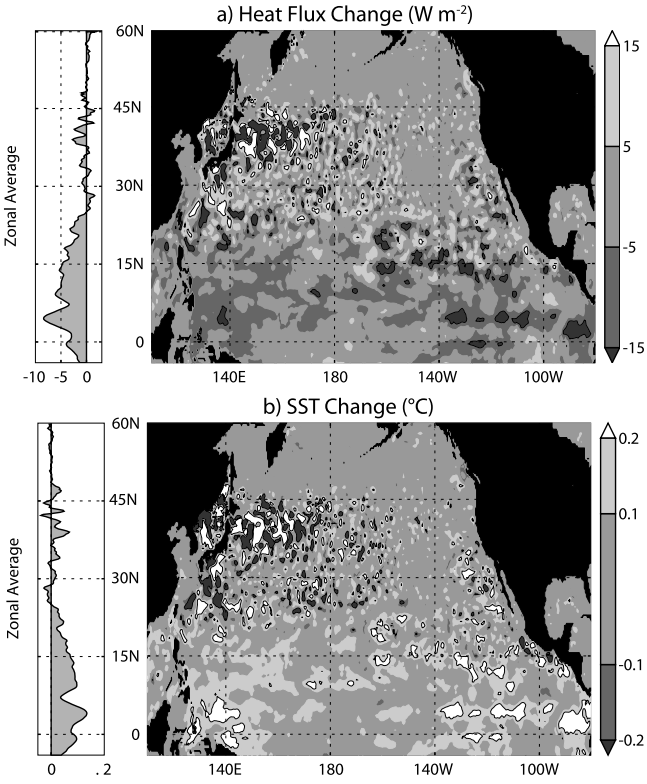

Figure 2. Average (a) latent plus sensible heat flux change (in W m^{-2}, positive values indicate warming of the ocean) and (b) sea surface temperature change (in °C) when the effect of ocean surface currents on the latent and sensible heat fluxes are included.

Extension. Stress changes are largest in the western tropical Pacific near 0° and 10°N, in the eastern tropics near 10°N, 105°W, and along the Kuroshio between 20°N and 30°N.

[14] Wind stress magnitude differences exceed 0.005 N m^{-2} in the tropics and 0.015 N m^{-2} over the center of the Kuroshio, with average strength differences of about 0.003 N m^{-2}. In the tropics and over the Kuroshio Extension, this amounts to no more than 5–10% of the mean wind stress strength; over the Kuroshio, this can be as much as 20%. Over most of the tropics, the wind stress is reduced, except for a zonal band of increased wind stress over the North Equatorial Countercurrent (NECC) between 5°N and 10°N. Wind stress curl changes were also calculated (not shown), but were found to be negligible except along the Kuroshio (not including the Extension) and between the large zonal bands of wind stress change in the tropics.

[15] As a result of the reduction in wind stress, surface current speeds are reduced by ~5 cm s^{-1} (~15%) over the tropics (Figure 1b), with the largest changes concentrated in the SEC and NECC. The westward intensification of the current changes near 5°N results from the tropical wind stress curl changes, which drive westward propagating Rossby waves. Velocity changes in the Kuroshio Extension are dominated by eddy field differences, and there is little organized surface current response outside of the tropics.

[16] Equatorial upwelling differences between the two runs are extremely noisy, but smoothing reveals a sizeable upwelling reduction between 170°W and 110°W, as well near the western boundary at 130°E (Figure 1c). This results in 3.9 Sv less upwelling in the equatorial Pacific (integrated across the basin between 2.5°S and 2.5°N) in the run with surface current effects versus the run without, representing a 16% reduction in model upwelling.

[17] Since surface currents tend to flow parallel to the mean wind, $|\mathbf{u}_a - \mathbf{u}_s|$ is typically smaller than $|\mathbf{u}_a|$ and thus one would expect inclusion of surface currents in the bulk formulas to reduce the heat flux magnitude (equations (1b) and (1c)). This reduction does occur in the Kuroshio (Figure 2a), but in the tropical Pacific south of 20°N, latent and sensible heat flux cooling actually increases by an average of 5 W m^{-2}, with peaks of ~15 W m^{-2}. Kuroshio Extension cooling also increases on average, although the spatial pattern there is dominated by eddy field differences between the two models. Evaporation increases over the tropics in much the same pattern as heat flux; since evaporation is just the latent heat flux divided by the latent heat of evaporation, we choose not to show evaporation here. (In Figure 2a, 15W m^{-2} roughly corresponds to 10 cm yr^{-1} of evaporation.)

[18] The increased cooling in the tropics occurs because tropical SST warms by ~0.1°C (Figure 2b) when surface currents are included in the bulk formulas, and the anomalously warm SST increases outgoing air-sea flux more than the weaker winds reduce it. The Kuroshio Extension SST also warms, but the field is again dominated by large eddy differences (~1°C). The SST variability in the Kuroshio Extension is enhanced relative to other surface fields in the area, due to the tight coupling between SST and heat flux through the bulk formulas.

[19] Power input by the wind decreases nearly everywhere (Figure 3), with the exception of the band of power increase along the NECC between 5°N and 10°N. Average power input in the tropics south of 20°N decreases by ~2 mW m^{-2}. Power decreases over the Kuroshio Extension also occur, but the Kuroshio Extension's relatively small area minimizes the impact of these changes on the basin's net power budget.

[20] Examining the basin-averaged flux changes relative to their mean values shows that the overall wind stress magnitude and heat flux change by 1–2% (Table 1).

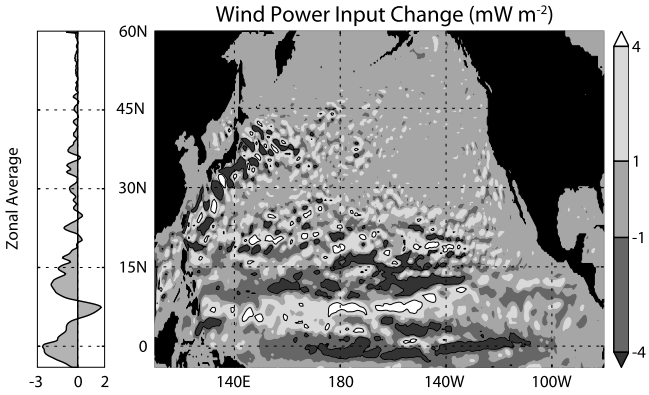

Figure 3. Wind power input change (in mW m^{-2}) when the effect of ocean surface currents on the wind stress is included.

Table 1. Area Averages of Wind Stress, Heat Flux, and Wind Power Input

	Without Currents	With Currents	Difference	% Change
Wind stress, mN m^{-2}	44	44	−0.4	−1%
Heat flux, W m^{-2}	−116	−118	−2.2	−2%
Geostrophic power (mW m^{-2}, 5°N–60°N)	1.13	0.83	−0.30	−27%
Ageostrophic power, mW m^{-2}				
Off-equatorial (5°N–60°N)	1.37	1.32	−0.05	−4%
Equatorial (5°S–5°N)	4.25	2.90	−1.35	−32%

Ageostrophic wind power input in the off-equatorial region is reduced by only 4%, since $\mathbf{u}_{geo}$, the surface geostrophic current, tends to project onto the wind stress better than $\mathbf{u}_{ageo}$, the surface ageostrophic current. Geostrophic wind power input, on the other hand, shows a reduction of 27% over the North Pacific. In the equatorial band (5S–5N), net wind power input is reduced 32%, but this is more difficult to interpret in the context of ocean power inputs, since there is no simple partition of energy input between the mixed layer and the general circulation near the equator, due to the breakdown of geostrophic dynamics.

4. Discussion

[21] We have calculated the impact of including the effect of surface currents in bulk formula calculations of air-sea momentum, heat, and fresh water fluxes in a high-resolution model of the North Pacific. Changes are concentrated over tropical ocean currents south of 20°N, in the Kuroshio path along the coast of Asia, and in the Kuroshio Extension between 30°N–40°N and 140°E–180°.

[22] The two year model spin up time creates issues in interpreting our results, since this is not long enough for the models to achieve proper equilibrium. This is likely only an issue in the midlatitudes, since the tropical ocean tends to adjust to forcing changes on a 1–2 year timescale. Furthermore, the bulk flux changes are concentrated in the tropics and over the boundary currents, suggesting that midlatitude adjustments will be minor relative to tropical adjustments. Actual estimates of the errors in our results due to continuing adjustment are difficult to make, due to the strong variability in the NCEP daily data and the short length of our integrations. However, further adjustment would likely increase the differences between the two models' SST and velocity fields, and so these results should probably be considered low estimates.

[23] Changes in wind stress, heat flux, and evaporation are minor when integrated over the basin, but in localized areas alter by 10–20% of the mean or more. Wind stress is reduced over most of the basin, resulting in ∼15% reductions in the speed of the SEC, NECC, and to a smaller extent, the NEC. Equatorial upwelling is also reduced by ∼15%, while heat flux to the atmosphere in the tropics increases by ∼5 W m^{-2}.

[24] Like *Luo et al.* [2005], we find equatorial SST increases when the effect of ocean currents on air-sea fluxes is included, although the warming in our model is only 20–50% of the value they found. Our smaller value may be partly explained by the brevity of the run we performed.

[25] The model's increase in both tropical SST and outgoing heat flux (Figure 2) is surprising, considering that increased heat flux to the atmosphere would tend to lower SST. It appears that including surface currents in the heat flux formulas (equations (1b) and (1c)) initially reduces heat flux out of the ocean (since $|\mathbf{u}_a - \mathbf{u}_s|$ is smaller than $|\mathbf{u}_a|$), causing SST to warm. However, warmer SST opposes the effect of reduced wind speed in the bulk formulas ($\theta_a - \theta_s$ and $q_a - q_s$ are generally negative, and become more negative as SST increases), increasing the outgoing heat flux. At the same time, reduced tropical upwelling (Figure 1c) causes less mixed layer entrainment cooling. This reduced cooling balances the increased outgoing heat flux, causing the system to reach a new equilibrium that has increased both SST and outgoing heat flux.

[26] In contrast to the small net wind stress and heat flux changes, wind power input is reduced by 27% when integrated over the basin. This is in good agreement with the 20–35% reduction calculated by *Duhaut and Straub* [2006] in their idealized model, and indicates the effect of surface currents must be taken into account in any calculations of wind power input to the general circulation. This has impacts outside of ocean modeling, since estimates of the wind power input to date have used wind stress climatologies that do not include this effect [*Oort et al.*, 1994; *Wunsch*, 1998; *Scott*, 1999]. The error in these calculations due to exclusion of surface current impacts on wind stress will be less than the 27% found in our model results, since reducing the model's wind stress also reduces the model's surface currents. Calculations using our model output suggest that using a wind stress that includes the effect of surface currents, without altering the surface currents themselves, results in a 15% net power reduction over 5°N–60°N. This suggests that scatterometer data, which naturally includes the effects of surface currents on wind stress, is an ideal data product with which to calculate wind energy input to the general circulation.

[27] **Acknowledgments.** We thank Kathie Kelly, Susan Hautala and two anonymous reviewers for their helpful comments on this paper. Figures were generated using the Matplotlib library in Python. This work was supported by NASA through the Ocean Vector Winds Science Team, JPL contract 1216233.

References

Chelton, D., M. G. Schlax, M. H. Freilich, and R. F. Milliff (2004), Satellite measurements reveal persistent small-scale features in ocean winds, *Science*, *303*, 978–983, doi:10.1126/science.1091901.

Cornillon, P., and K.-A. Park (2001), Warm core ring velocities inferred from NSCAT, *Geophys. Res. Lett.*, *28*, 575–578.

Duhaut, T. H. A., and D. N. Straub (2006), Wind stress dependence on ocean surface velocity: Implications for mechanical energy input to ocean circulation, *J. Phys. Oceanogr.*, *36*(2), 202–211.

Fairall, C. W., et al. (1996), Bulk parameterization of air-sea fluxes for Tropical Ocean-Global Atmosphere Couple-Ocean Atmosphere Response Experiment, *J. Geophys. Res.*, *101*(C2), 3747–3764.

Hallberg, R. (1995), Some aspects of the circulation in ocean basins with isopycnals intersecting the sloping boundaries, Ph.D. thesis, 244 pp., Univ. of Wash., Seattle.

Kelly, K., et al. (2001), Ocean currents evident in satellite wind data, *Geophys. Res. Lett.*, *28*, 2469–2472.

Ladd, C. A., and L. Thompson (2002), Decadal variability of North Pacific Central Mode Water, *J. Phys. Oceanogr.*, *32*, 2870–2881, doi:10.1175/1520-0485(2002)032<2870:DVONPC>2.0.CO;2.

Large, W. S., and S. Pond (1982), Sensible and latent heat flux measurements over the ocean, *J. Phys. Oceanogr.*, *12*, 464–482.

Luo, J.-J., et al. (2005), Reducing climatology bias in an ocean-atmosphere CGCM with improved coupling physics, *J. Clim.*, *18*, 2344–2360.

Munk, W., and C. Wunsch (1998), Abyssal recipes II: Energetics of tidal and wind mixing, *Deep Sea Res., Part I*, *45*, 1977–2010.

Oberhuber, J. M. (1993), Simulation of the Atlantic circulation with a coupled sea ice-mixed layer-isopycnal general circulation model. Part I: Model description, *J. Phys. Oceanogr.*, *23*, 808–829.

Oort, A. H., L. A. Anderson, and J. P. Peixoto (1994), Estimates of the energy cycle of the oceans, *J. Geophys. Res.*, *99*(C4), 7665–7688.

Pacanowski, R. C. (1987), Effect of equatorial currents on surface stress, *J. Phys. Oceanogr.*, *17*, 833–838.

Scott, R. B. (1999), Mechanical energy flux to the surface geostrophic flow using TOPEX/Poseidon data, *Phys. Chem. Earth, Part A*, *24*, 399–402.

Wang, W., and R. X. Huang (2004), Wind energy input to the Ekman layer, *J. Phys. Oceanogr.*, *34*, 1267–1275.

Wunsch, C. (1998), The work done by wind on the oceanic general circulation, *J. Phys. Oceanogr.*, *28*, 2332–2340.

Zeng, X., M. Zhao, and R. E. Dickinson (1998), Intercomparison of bulk aerodynamic algorithms for the computation of sea surface fluxes using TOGA COARE and TAO data, *J. Clim.*, *11*, 2628–2644.

J. T. Dawe and L. Thompson, Department of Oceanography, University of Washington, Box 355351, Seattle, WA 98195, USA. (freedryk@ocean.washington.edu)